ISSN: 1392-6292/ eISSN: 1648-3510

VILNIUS TECH
Vilnius Gediminas Technical University

MATHEMATICAL MODELLING and ANALYSIS

2026
Volume 31
Issue 2
Pages 303–325
https://doi.org/10.3846/mma.2026.24728

Efficient spectral-Galerkin method for the two-dimensional Gray-Scott model

Yujian Jiao ✉ and Mengshu Jia

Department of Mathematics, Shanghai Normal University, 200234 Shanghai, China

Article History:

- received August 31, 2025
- revised December 31, 2025
- accepted February 3, 2026

Abstract. The Gray-Scott (GS) model is a nonlinear reaction diffusion system widely used in applied sciences. This paper delves into the investigation of a spectral method for the GS model with homogeneous Neumann boundary conditions. The proposed numerical scheme integrates a spectral approach based on generalized Jacobi polynomials for spatial discretization with the two-step backward differentiation formula (BDF2) for temporal discretization. We prove the boundedness, generalized stability, and convergence of this new method. Extensive numerical results demonstrate the efficiency of the new proposed scheme and provide numerical validation of the theoretical analysis. The key advantages of our new approach are twofold: (i) it utilizes generalized Jacobi polynomials with indices $\alpha = \beta = -2$, which naturally satisfy the boundary conditions and thereby not only simplify the theoretical analysis but also yield a well-conditioned discrete system that enhances computational efficiency; and (ii) the numerical errors exhibit exponential decay in space.

Keywords: spectral method; Gray-Scott model; generalized Jacobi polynomials; nonlinear system; reaction-diffusion system.

AMS Subject Classification: 33C45; 35K57; 35B36; 65L60; 65L70.

✉ Corresponding author. E-mail: yj-jiao@shnu.edu.cn

1 Introduction

Let $\Omega \subset R^2$ is a bounded domain, $T > 0$. The GS model is the following reaction-difusion system in dimensionless units [7]:

$$\begin{cases} \dfrac{\partial u}{\partial t} = d_u \nabla^2 u + F(1-u) - uv^2, & \text{in } \Omega \times (0,T), \\ \dfrac{\partial v}{\partial t} = d_v \nabla^2 v - (F+k)v + uv^2, & \text{in } \Omega \times (0,T), \end{cases} \tag{1.1}$$

where u and v are concentrations of the chemical materials U and V, respectively, d_u and d_v the diffusion coefficients, F the in-flow rate of U from outside, k the removal rate of V from reaction field. Due to its effectiveness in describing self-organizing phenomena and pattern formation, it has been widely used in fluids, semiconductors, biology, chemistry, and other fields [6, 13, 16].

The mechanism, existence, stability, and types of pattern formation in the GS model have attracted considerable attention. Nishiura and Ueyama [17] analyzed self-replicating patterns from a global bifurcation perspective. Wei and Winter [23] rigorously established the existence and stability of multiple-spot solutions in two dimensions. McGough and Riley [14] confirmed nonuniform steady-state solutions via bifurcation analysis. Kolokolnikov et al. [12] constructed equilibrium stripe solutions and studied the stability of stripes and rings under zigzag and breakup instabilities. Wang et al. [22] investigated the effects of noise and time-dependent diffusivity on pattern formation in an extended Gray–Scott model. Castelli [4] combined analytical and numerical methods to demonstrate the existence of various nonhomogeneous stationary patterns on bounded domains.

The nonlinearity of the GS model makes it difficult to find analytical solutions, leading to extensive research on numerical methods. Zegeling and Kok [25] proposed an adaptive moving mesh approach, while Abbaszadeh and Dehghan [1] developed a fast reduced-order finite difference scheme with ADI and POD for the space-fractional model. Dehghan et al. [5] employed an element-free Galerkin method with a fourth-order exponential time-differencing Runge–Kutta scheme. Yadav and Jiwari [24] established well-posedness and constructed Galerkin finite element approximations using the Crank–Nicolson scheme. Amin and Mashat [3] applied finite difference and finite volume methods to two-dimensional simulations. Singh et al. [18] employed a mixed modal discontinuous Galerkin method with a TVD Runge–Kutta scheme to study multi-dimensional pattern formation. More recently, Abbaszadeh et al. [2] proposed a POD-based reduced-order spectral Galerkin method with rigorous error estimates.

In this work, we propose a spectral method using the generalised Jacobi polynomials for the two-dimensional GS model (1.1) with optimal error analysis. The generalized Jacobi polynomials $j_n^{-2,-2}(x), n \geq 4$ satisfies the boundary conditions $j_n^{-2,-2}(\pm 1) = \frac{dj_n^{-2,-2}(x)}{dx}|_{x=\pm 1} = 0$ and therefore require no compact combinations to enforce boundary conditions, unlike Legendre or Chebyshev polynomials. Hence, the set $\{j_n^{-2,-2}(x)\}$ serves as a natural basis for problem (3.1). Their use leads to a significantly simplified analysis, sharper error estimates, and well-conditioned numerical algorithms. After the spatial discretization, we employ the BDF2 scheme to integrate the resulting system of ordinary differential equations. We have established the boundedness, generalized stability, and convergence of the numerical solution.

The paper is structured as follows. In the next section, we recall some properties of the generalized Jacobi polynomials and derive some approximation results. In Section 3, we propose a spectral method for the two-dimensional GS model and prove the boundedness of the numerical solution. Section 4 is devoted to the error analysis. In Section 5, we present the details of numerical implementation and some numerical results to validate the efficiency of our new algorithm. The final section is for concluding discussion.

2 Preliminaries

In this section, we show some results on the generalised Jacobi polynomials that will be used in the upcoming discussion. Let $I = \{z \mid |z| < 1\}$, $\partial_z v(z) = \frac{\partial}{\partial z} v(z)$, and $\chi(z)$ be a certain weight function. For an integer $\mu \geq 0$, we denote by $(u, v)_{\mu,\chi,I}$, $|u|_{\mu,\chi,I}$ and $\|u\|_{\mu,\chi,I}$ the inner product, semi-norm and norm of space $H^{\mu}_{\chi}(I)$, respectively. In particular, $H^0_{\chi}(I) = L^2_{\chi}(I)$ has inner product $(u, v)_{\chi,I}$ and the norm $\|u\|_{\chi,I}$. For simplicity, we omit the subscript χ whenever $\chi(z) \equiv 1$.

Let $\alpha, \beta > -1$ and $\chi^{\alpha,\beta}(z) = (1-z)^{\alpha}(1+z)^{\beta}$ be a weight function. The nth-order Jacobi polynomial defined on I denoted by $p_n^{\alpha,\beta}(z)$. The set of $\{p_n^{\alpha,\beta}(z)\}$ is mutually orthogonal with respect to the weight $\chi^{\alpha,\beta}(z)$, namely

$$(p_n^{\alpha,\beta}(z), p_{n'}^{\alpha,\beta}(z))_{\chi^{\alpha,\beta}(z)} = \gamma_n^{\alpha,\beta}\delta_{n,n'}, \tag{2.1}$$

where $\delta_{n,n'}$ is the Kronecker Delta symbol, and

$$\gamma_n^{\alpha,\beta} = \frac{2^{\alpha+\beta+1}\Gamma(n+\alpha+1)\Gamma(n+\beta+1)}{(2n+\alpha+\beta+1)n!\Gamma(n+\alpha+\beta+1)}.$$

In particular, $L_n(z) = p_n^{0,0}(z)$ be the Legendre polynomial.

We introduce polynomial

$$\psi_n(z) = \frac{1}{(n-2)(n-3)}(1-z^2)^2 p_{n-4}^{(2,2)}(z), \quad n \geq 4.$$

In fact, the polynomial $(n-2)(n-3)\psi_n(z)$ is precisely the generalized Jacobi polynomial $j_n^{-2,-2}(z)$ given in [8]. The combination of (B.8) and (B.9) of [8] gives

$$\begin{aligned}\psi_n(z) =& \frac{4}{(2n-3)(2n-5)}(L_{n-4}(z) - \frac{2(2n-3)}{2n-1}L_{n-2}(z) \\ &+ \frac{2n-5}{2n-1}L_n(z)), \ n \geq 4,\end{aligned} \tag{2.2}$$

$$\partial_z\psi_n(z) = -\frac{4}{2n-3}(L_{n-3}(z) - L_{n-1}(z)), \quad n \geq 3. \tag{2.3}$$

Furthermore, we have

$$\int_I \partial_z^k\psi_n(z)\partial_z^k\psi_{n'}(z)(1-z^2)^{k-2}dz = E_{n,k}\delta_{n,n'}, \quad k \leq n-1, 4 \leq n,$$

where

$$E_{n,k} = \frac{32(n+k-4)}{(2n-3)(n-k)!}, \quad k \leq n, \quad n \geq 4.$$

Obviously, $\partial_z^k\psi_n(z) = 0$ for $4 \leq n < k$. For any non-negative integer N, we set $\hat{\mathcal{V}}_N(I) = \text{span}\{\psi_n(z) \mid 4 \leq n \leq N\}$. Let $\xi_z = 1-z^2$. The $L^2_{\xi_z^{-2}}$−orthogonal projection $\Pi_{N,I} : L^2_{\xi_z^{-2}}(I) \to \hat{\mathcal{V}}_N(I)$ defined by $(\Pi_{N,I}v - v, \psi)_{L^2_{\xi_z^{-2}}(I)} = 0, \quad \forall\psi \in \hat{\mathcal{V}}_N(I)$.

Lemma 1. *(Lemma 2.2 of [10])If* $v \in L^2_{\xi_z^{-2}}(I)$, $\partial_z^r v \in L^2_{\xi_z^{r-2}}(I)$, *for integers* $N \geq 4$, $1 \leq r \leq N+1$, $0 \leq \mu \leq r$, *then,*

$$\|\partial_z^\mu \left(\Pi_{N,I} v - v\right)\|_{L^2_{\xi_z^{\mu-2}}(I)} \leq c N^{\mu-r} \|\partial_z^r v\|_{L^2_{\xi_z^{r-2}}(I)}.$$

Let $I_z = \{z \mid |z| < 1\}$, $\boldsymbol{z} = (x, y)$. Denote $\Omega = I_x \otimes I_y$ with the boundary $\partial\Omega$ and $\bar{\Omega} = \Omega \cup \partial\Omega$, and $\boldsymbol{n}$ is the unit outward norm on Ω. Denote $\xi_{xy}(\boldsymbol{z}) = (1-x^2)(1-y^2)$. For any scalar function $v(\boldsymbol{z})$, we introduce the space

$$L^2_{\xi_{xy}^{-2}}(\Omega) = \{v(\boldsymbol{z}) \mid v(\boldsymbol{z}) \text{ is measurable and } \|v\|_{L^2_{\xi_{xy}^{-2}}(\Omega)} < \infty\},$$

with the inner product and norm

$$(u, v)_{L^2_{\xi_{xy}^{-2}}(\Omega)} = \int_\Omega u(\boldsymbol{z}) v(\boldsymbol{z}) \xi_{xy}^{-2}(\boldsymbol{z}) d\boldsymbol{z}, \quad \|v\|_{L^2_{\xi_{xy}^{-2}}(\Omega)} = (v, v)^{\frac{1}{2}}_{L^2_{\xi_{xy}^{-2}}(\Omega)}.$$

In addition, the space $H^1(\Omega)$ is as usual.

Let $\phi_{n_1,n_2}(\boldsymbol{z}) = \psi_{n_1}(x)\psi_{n_2}(y)$, $n_1, n_2 \geq 4$. The set of $\{\phi_{n_1,n_2}(\boldsymbol{z})\}$ constitutes a complete orthogonal system, namely

$$\int_\Omega \phi_{n_1,n_2}(\boldsymbol{z}) \phi_{n_1',n_2'}(\boldsymbol{z}) \xi_{xy}^{-2}(\boldsymbol{z}) d\boldsymbol{z} = \zeta_{n_1,n_2} \delta_{n_1,n_1'} \delta_{n_2,n_2'}, \tag{2.4}$$

where $\zeta_{n_1,n_2} = E_{n_1,0} E_{n_2,0}$. We set

$$\hat{\mathcal{V}}_N(\Omega) = \text{span}\{\phi_{n_1,n_2}(\boldsymbol{z}) \mid 4 \leq n_1 \leq N,\ 4 \leq n_2 \leq N\}.$$

The orthogonal projection $\Pi_{N,\Omega} : L^2_{\xi_{xy}^{-2}}(\Omega) \to \hat{\mathcal{V}}_N(\Omega)$ is defined by

$$\left(\Pi_{N,\Omega} v - v, \phi_{n_1,n_2}\right)_{\xi_{xy}^{-2}} = 0, \quad \forall \phi_{n_1,n_2} \in \hat{\mathcal{V}}_N(\Omega).$$

Lemma 2. *(Theorem 3.1 of [19]) If* $v \in L^2_{\xi_{xy}^{-2}}(\Omega)$, *for integers* $N \geq 4$, $0 \leq \nu_\sigma \leq r_\sigma \leq N+1$, $\xi_\sigma^{\frac{r_\sigma}{2}} \xi_\sigma^{\frac{\nu_\sigma}{2}} \partial_\sigma^{\nu_\sigma} \partial_\sigma^{r_\sigma} v \in L^2_{\xi_{xy}^{-2}}(\Omega)$, $\sigma = x, y$, *then, we have*

$$\begin{aligned}
&\left\|\partial_x^{\nu_x} \partial_y^{\nu_y} (\Pi_{N,\Omega} v - v)\right\|_{L^2_{\xi_x^{-2+\nu_x} \xi_y^{-2+\nu_y}}(\Omega)} \\
&\leq c\Big(N^{\nu_x - r_x} \left\|\partial_x^{r_x} \partial_y^{\nu_y} v\right\|_{L^2_{\xi_x^{r_x-2} \xi_y^{r_x-2}}\left(I_x; L^2_{\xi_x^{\nu_y-2} \xi_y^{\nu_y-2}}(I_y)\right)} \\
&\quad + N^{\nu_y - r_y} \left\|\partial_x^{\nu_x} \partial_y^{r_y} v\right\|_{L^2_{\xi_x^{\nu_x-2} \xi_y^{\nu_x-2}}\left(I_x; L^2_{\xi_x^{r_y-2} \xi_y^{r_y-2}}(I_y)\right)}\Big).
\end{aligned}$$

Next, we proceed to derive some approximation results for the two-dimensional vector function space. Let

$$\boldsymbol{\xi}_{xy}(\boldsymbol{z}) = \left(\xi_{xy}(\boldsymbol{z}), \xi_{xy}(\boldsymbol{z})\right)^T, \quad \boldsymbol{\phi}_{n_1,n_2}(\boldsymbol{z}) = \left(\phi_{n_1,n_2}(\boldsymbol{z}), \phi_{n_1,n_2}(\boldsymbol{z})\right)^T.$$

For any vector function $\boldsymbol{w}(\boldsymbol{z}) = \big(u(\boldsymbol{z}), v(\boldsymbol{z})\big)^T$, we define space

$$\boldsymbol{\mathcal{V}}(\Omega) = \{\boldsymbol{w}(\boldsymbol{z}) \mid u(\boldsymbol{z}), v(\boldsymbol{z}) \in L^2_{\xi_{xy}^{-2}}(\Omega) \text{ and } \frac{\partial \boldsymbol{w}}{\partial \boldsymbol{n}} = 0 \text{ on } \partial\Omega\}.$$

Then, for any $\boldsymbol{w}(\boldsymbol{z}) \in \boldsymbol{\mathcal{V}}(\Omega)$,

$$\begin{cases} u(\boldsymbol{z}) = \displaystyle\sum_{n_1=4}^{\infty}\sum_{n_2=4}^{\infty} \hat{u}_{n_1,n_2}\phi_{n_1,n_2}(\boldsymbol{z}), \\ v(\boldsymbol{z}) = \displaystyle\sum_{n_1=4}^{\infty}\sum_{n_2=4}^{\infty} \hat{v}_{n_1,n_2}\phi_{n_1,n_2}(\boldsymbol{z}), \end{cases} \tag{2.5}$$

where

$$\hat{u}_{n_1,n_2} = \frac{1}{E_{n_1,0}E_{n_2,0}}\int_{\Omega} \xi_{xy}^{-2}(\boldsymbol{z})u(\boldsymbol{z})\phi_{n_1,n_2}(\boldsymbol{z})d\boldsymbol{z},$$
$$\hat{v}_{n_1,n_2} = \frac{1}{E_{n_1,0}E_{n_2,0}}\int_{\Omega} \xi_{xy}^{-2}(\boldsymbol{z})v(\boldsymbol{z})\phi_{n_1,n_2}(\boldsymbol{z})d\boldsymbol{z}.$$

Denote $\mathbf{L}^2_{\boldsymbol{\xi}_{xy}^{-2}}(\Omega) = \big(L^2_{\xi_{xy}^{-2}}(\Omega), L^2_{\xi_{xy}^{-2}}(\Omega)\big)^T$ and $\hat{\boldsymbol{\mathcal{V}}}_N(\Omega) = \hat{\mathcal{V}}_N(\Omega) \otimes \hat{\mathcal{V}}_N(\Omega)$. The orthogonal projection $\boldsymbol{\Pi}_{N,\Omega} : \mathbf{L}^2_{\boldsymbol{\xi}_{xy}^{-2}}(\Omega) \to \hat{\boldsymbol{\mathcal{V}}}_N(\Omega)$ is defined by

$$(\boldsymbol{\Pi}_{N,\Omega}\boldsymbol{w} - \boldsymbol{w}, \boldsymbol{\phi}_{n_1,n_2})_{\mathbf{L}^2_{\boldsymbol{\xi}_{xy}^{-2}}(\Omega)} = 0, \quad \forall \boldsymbol{\phi}_{n_1,n_2} \in \hat{\boldsymbol{\mathcal{V}}}_N(\Omega).$$

Let

$$\boldsymbol{w}_N^*(\boldsymbol{z}) = \big(\Pi_{N,I_x} \circ \Pi_{N,I_y} u(\boldsymbol{z}),\ \Pi_{N,I_x} \circ \Pi_{N,I_y} v(\boldsymbol{z})\big)^T.$$

Lemma 3. *For any $\boldsymbol{w}(\boldsymbol{z}) \in \boldsymbol{\mathcal{V}}(\Omega)$, we have*

$$\boldsymbol{\Pi}_{N,\Omega}\boldsymbol{w}(\boldsymbol{z}) = \boldsymbol{w}_N^*(\boldsymbol{z}). \tag{2.6}$$

Proof. According to the definition of $\Pi_{N,\Omega}$ and (2.5), we have that for any $\boldsymbol{w}(\boldsymbol{z}) \in \boldsymbol{\mathcal{V}}(\Omega)$,

$$\begin{cases} u_N^*(\boldsymbol{z}) = \Pi_{N,I_x} \circ \Pi_{N,I_y}\big(\displaystyle\sum_{n_1=4}^{\infty}\sum_{n_2=4}^{\infty} \hat{u}_{n_1,n_2}\phi_{n_1,n_2}(\boldsymbol{z})\big) \\ \qquad\quad = \displaystyle\sum_{n_1=4}^{N}\sum_{n_2=4}^{N} \hat{u}_{n_1,n_2}\psi_{n_1}(x)\psi_{n_2}(y), \\ v_N^*(\boldsymbol{z}) = \Pi_{N,I_x} \circ \Pi_{N,I_y}\big(\displaystyle\sum_{n_1=4}^{\infty}\sum_{n_2=4}^{\infty} \hat{v}_{n_1,n_2}\phi_{n_1,n_2}(\boldsymbol{z})\big) \\ \qquad\quad = \displaystyle\sum_{n_1=4}^{N}\sum_{n_2=4}^{N} \hat{v}_{n_1,n_2}\psi_{n_1}(x)\psi_{n_2}(y). \end{cases} \tag{2.7}$$

Therefore, $\boldsymbol{w}_N^*(\boldsymbol{z}) \in \hat{\boldsymbol{\mathcal{V}}}_N(\Omega)$ and $\frac{\partial \boldsymbol{w}_N^*}{\partial \boldsymbol{n}} = 0$ on $\partial\Omega$. Thanks to (2.5) and (2.7), we get

$$\begin{cases} u(\boldsymbol{z}) - u_N^*(\boldsymbol{z}) = \displaystyle\sum_{n_1=N+1}^{\infty} \sum_{n_2=N+1}^{\infty} \hat{u}_{n_1,n_2} \boldsymbol{\phi}_{n_1,n_2}(\boldsymbol{z}), \\ v(\boldsymbol{z}) - v_N^*(\boldsymbol{z}) = \displaystyle\sum_{n_1=N+1}^{\infty} \sum_{n_2=N+1}^{\infty} \hat{v}_{n_1,n_2} \boldsymbol{\phi}^{(2)}_{n_1,n_2}(\boldsymbol{z}). \end{cases}$$

By (2.4), we have

$$\left(\boldsymbol{w} - \boldsymbol{w}_N^*, \boldsymbol{\phi}_{n_1,n_2}\right)_{\mathbf{L}^2_{\boldsymbol{\xi}_{xy}^{-2}}(\Omega)} = 0, \quad \forall \boldsymbol{\phi}_{n_1,n_2} \in \hat{\boldsymbol{\mathcal{V}}}_N(\Omega).$$

Then, we get the desired result (2.6). □

To describe the approximation error, we introduce the quantity

$$\begin{aligned} A_r(\boldsymbol{w}) =& \|\partial_x^r u\|_{L^2_{\xi_{xy}^{r-2}}(I_x;L^2_{\xi_{xy}^{-2}}(I_y))} + \|\partial_y^r u\|_{L^2_{\xi_{xy}^{-2}}(I_x;L^2_{\xi_{xy}^{r-2}}(I_y))} \\ &+ \|\partial_x^r v\|_{L^2_{\xi_{xy}^{r-2}}(I_x;L^2_{\xi_{xy}^{-2}}(I_y))} + \|\partial_y^r v\|_{L^2_{\xi_{xy}^{-2}}(I_x;L^2_{\xi_{xy}^{r-2}}(I_y))}. \end{aligned}$$

Lemma 4. *If $\boldsymbol{w} \in \boldsymbol{\mathcal{V}}(\Omega)$ and $A_r(\boldsymbol{w})$ is finite, integers $N \geq 4$, $0 \leq r \leq N+1$. Then,*

$$\|\boldsymbol{\Pi}_{N,\Omega}\boldsymbol{w} - \boldsymbol{w}\|_{\mathbf{L}^2_{\boldsymbol{\xi}_{xy}^{-2}}(\Omega)} \leq cN^{-r} A_r(\boldsymbol{w}). \tag{2.8}$$

Proof. According to Lemma 3, we have

$$\boldsymbol{\Pi}_{N,\Omega}\boldsymbol{w} - \boldsymbol{w} = \boldsymbol{w}_N^* - \boldsymbol{w} = (\Pi_{N,\Omega}u - u, \Pi_{N,\Omega}v - v)^T.$$

Then,

$$\|\boldsymbol{\Pi}_{N,\Omega}\boldsymbol{w} - \boldsymbol{w}\|^2_{\mathbf{L}^2_{\boldsymbol{\xi}_{xy}^{-2}}(\Omega)} = \|\Pi_{N,\Omega}u - u\|^2_{L^2_{\xi_{xy}^{-2}(\Omega)}} + \|\Pi_{N,\Omega}v - v\|^2_{L^2_{\xi_{xy}^{-2}(\Omega)}}.$$

Then, by Lemma 2 we can get the desired result (2.8). □

We introduce space $\mathbf{L}^2(\Omega) = \left(L^2(\Omega)\right)^2$. For any $\boldsymbol{w}, \boldsymbol{u} \in \mathbf{L}^2(\Omega)$, the inner product and norm are defined by

$$(\boldsymbol{w}, \boldsymbol{u})_{\mathbf{L}^2(\Omega)} = \sum_{i=1}^{2} (w_i, u_i)_{L^2(\Omega)}, \qquad \|\boldsymbol{w}\|_{\mathbf{L}^2(\Omega)} = (\boldsymbol{w}, \boldsymbol{w})^{\frac{1}{2}}_{\boldsymbol{L}^2(\Omega)},$$

respectively. For any nonnegative integer r, we define space $\mathbf{H}^r(\Omega) = \left(H^r(\Omega)\right)^2$, equipped with the inner product $(\boldsymbol{w}, \boldsymbol{u})_{\mathbf{H}^r(\Omega)}$, semi-norm $|\boldsymbol{w}|_{\mathbf{H}^r(\Omega)}$, and norm $\|\boldsymbol{w}\|_{\mathbf{H}^r(\Omega)}$. Denote $\hat{H}^{1,0}(\Omega) = \{v(\boldsymbol{z}) \mid v(\boldsymbol{z}) \in H^1(\Omega) \text{ and } \frac{\partial v}{\partial \boldsymbol{n}} = 0 \text{ on } \partial\Omega\}$, and

$\boldsymbol{\mathcal{H}}(\Omega)=\big(\hat{H}^{1,0}(\Omega)\big)^2$. Let $\boldsymbol{\mathcal{V}}_N(\Omega)=\hat{\boldsymbol{\mathcal{V}}}_N(\Omega)\cap\boldsymbol{\mathcal{H}}(\Omega)$. The orthogonal projection $\boldsymbol{\Pi}^{1,0}_{N,\Omega}:\boldsymbol{\mathcal{H}}(\Omega)\to\boldsymbol{\mathcal{V}}_N(\Omega)$ is a mapping such that for $\forall\ \boldsymbol{w}(\boldsymbol{z})\in\boldsymbol{\mathcal{H}}(\Omega)$

$$\Big(\nabla\big(\boldsymbol{\Pi}^{1,0}_{N,\Omega}\boldsymbol{w}(\boldsymbol{z})-\boldsymbol{w}(\boldsymbol{z})\big),\nabla\boldsymbol{\phi}(\boldsymbol{z})\Big)=0,\quad\forall\ \boldsymbol{\phi}(\boldsymbol{z})\in\boldsymbol{\mathcal{V}}_N(\Omega).$$

For describing the approximation error of $\boldsymbol{\Pi}^{1,0}_{N,\Omega}$, we introduce the space $B_r(\boldsymbol{w})$ endowed the norm

$$\begin{aligned}B_r(u)=&\|\partial_x^r u\|_{L^2_{\xi_x^{r-1}\xi_x^{r-2}}(I_x;L^2_{\xi_x^{-1}\xi_y^{-2}}(I_y))}+\|\partial_y^r u\|_{L^2_{\xi_x^{-1}\xi_y^{-2}}(I_x;L^2_{\xi_x^{r-1}\xi_y^{r-2}}(I_y))}\\&+\|\partial_x^r u\|_{L^2_{\xi_x^{r-2}\xi_{xy}^{r-1}}(I_x;L^2_{\xi_x^{-2}\xi_y^{-1}}(I_y))}+\|\partial_y^r u\|_{L^2_{\xi_x^{-2}\xi_y^{-1}}(I_x;L^2_{\xi_x^{r-2}\xi_y^{r-1}}(I_y))}.\end{aligned}$$

Denote $B_r(\boldsymbol{w})=B_r(u)+B_r(v)$.

Lemma 5. *If $\boldsymbol{w}(\boldsymbol{z})\in\boldsymbol{\mathcal{H}}(\Omega)$, $B_r(\boldsymbol{w})$ is finite, integers $N\geq 4$, $1\leq r\leq N+1$, then,*

$$\big\|\boldsymbol{\Pi}^{1,0}_{N,\Omega}\boldsymbol{w}-\boldsymbol{w}\big\|_{\mathbf{H}^1(\Omega)}\leq cN^{1-r}B_r(\boldsymbol{w}).\tag{2.9}$$

Proof. According to the proof of Lemma 3, we get $\boldsymbol{w}_N^*\in\boldsymbol{\mathcal{V}}_N(\Omega)$. By the projection theorem we have

$$\big\|\boldsymbol{\Pi}^{1,0}_{N,\Omega}\boldsymbol{w}-\boldsymbol{w}\big\|_{\mathbf{H}^1(\Omega)}=\inf_{\boldsymbol{\phi}\in\boldsymbol{\mathcal{V}}_N(\Omega)}\|\boldsymbol{\phi}-\boldsymbol{w}\|_{\mathbf{H}^1(\Omega)}\leq\|\boldsymbol{w}_N^*-\boldsymbol{w}\|_{\mathbf{H}^1(\Omega)}.$$

Obviously,

$$\big|\boldsymbol{w}_N^*-\boldsymbol{w}\big|_{\mathbf{H}^1(\Omega)}=\big\|\nabla\big(\Pi_{N,\Omega}u-u\big)\big\|_{L^2(\Omega)}+\big\|\nabla\big(\Pi_{N,\Omega}v-v\big)\big\|_{L^2(\Omega)}.$$

According to $\xi_x^{-1}\xi_y^{-2}>1$ and $\xi_x^{-2}\xi_y^{-1}>1$, Lemma 2 with $\nu_x=1$, $\nu_y=0$, and $\nu_x=0$, $\nu_y=1$ and Poincaré inequality, we arrive at the desired result (2.9). □

In the forthcoming discussion, the following inequality plays an important role.

Lemma 6. *For any $\boldsymbol{\phi}\in\hat{\boldsymbol{\mathcal{V}}}_N(\Omega)$, $1\leq p\leq q\leq\infty$, then,*

$$\|\boldsymbol{\phi}\|_{\mathbf{L}^q(\Omega)}\leq((p+1)N^2)^{\frac{1}{p}-\frac{1}{q}}\|\boldsymbol{\phi}\|_{\mathbf{L}^p(\Omega)}.$$

In the error analysis we need also the following inequality.

Lemma 7. *For any $\boldsymbol{w}\in\boldsymbol{\mathcal{V}}(\Omega)$,*

$$\|\boldsymbol{w}\|^2_{\mathbf{L}^4(\Omega)}\leq c\|\boldsymbol{w}\|_{\mathbf{L}^2(\Omega)}|\boldsymbol{w}|_{\mathbf{H}^1(\Omega)}.\tag{2.10}$$

Lemma 8. *(cf. Lemma 4.1 of [9]). Assume that*
(i) d and d_k are non-negative constants,
(ii) $\mathcal{E}(\eta)$ is a non-negative function of η,
(iii) $\rho\geq 0$ and for all $0\leq\eta\leq\eta_1$,

$$\mathcal{E}(\eta)\leq\rho+d\int_0^\eta\big(\mathcal{E}(\zeta)+\sum_{k=2}^n N^{d_k}\mathcal{E}^k(\zeta)\big)d\zeta,$$

(iv) for certain $\eta_1 > 0$, $\rho e^{d_n \eta_1} \le \min\limits_{2\le k\le n} N^{-d_k/(k-1)}$.

Then, for all $0 \le \eta \le \eta_1$,

$$\mathcal{E}(\eta) \le \rho e^{d_n \eta}.$$

3 Spectral scheme

In this section, we study a spectral scheme for (1.1) with homogeneous Neumann boundary conditions $\frac{\partial \boldsymbol{w}}{\partial \boldsymbol{n}} = 0$ on $\partial\Omega$ and analyze it's boundedness.

The vector function form of the system (1.1) with homogeneous Neumann boundary conditions is as follows

$$\begin{cases} \partial_t \boldsymbol{w} = d\nabla^2 \boldsymbol{w} + W(\boldsymbol{w}) + R(\boldsymbol{w}), & \text{in } \Omega \times (0,T), \\ \dfrac{\partial \boldsymbol{w}}{\partial \boldsymbol{n}} = 0, & \text{on } \partial\Omega \times [0,T], \\ \boldsymbol{w}(\boldsymbol{z},0) = \boldsymbol{w}_0(\boldsymbol{z}), & \text{in } \Omega, \end{cases} \tag{3.1}$$

where

$$d\nabla^2 \boldsymbol{w} = \big(d_u \nabla^2 u,\ d_v \nabla^2 v\big)^T, \quad W(\boldsymbol{w}) = \big(F(1-u),\ -(F+k)v\big)^T,$$
$$R(\boldsymbol{w}) = \big(-uv^2,\ uv^2\big)^T.$$

We define space $\boldsymbol{\mathcal{L}}(\Omega) = \{\boldsymbol{w} \mid \boldsymbol{w} \in \mathbf{L}^2(\Omega),\ \frac{\partial \boldsymbol{w}}{\partial \boldsymbol{n}} = 0 \text{ on } \partial\Omega\}$. The weak form of (3.1) is to find $\boldsymbol{w} \in H^1(0,T;\boldsymbol{\mathcal{L}}(\Omega)) \cap L^\infty(0,T;\boldsymbol{\mathcal{H}}(\Omega))$, such that

$$\begin{cases} (\partial_t \boldsymbol{w}, \boldsymbol{h}) + d(\nabla \boldsymbol{w}, \nabla \boldsymbol{h}) = (W(\boldsymbol{w}), \boldsymbol{h}) + (R(\boldsymbol{w}), \boldsymbol{h}),\ \forall \boldsymbol{h} \in \boldsymbol{\mathcal{H}}(\Omega),\ 0 < t \le T, \\ \boldsymbol{w}(\boldsymbol{z},0) = \boldsymbol{w}_0(\boldsymbol{z}), \quad \boldsymbol{z} \in \bar{\Omega}. \end{cases} \tag{3.2}$$

Then, the spectral scheme of (3.2) is to seek $\boldsymbol{w}_N(t) = (u_N(t), v_N(t))^T \in \boldsymbol{\mathcal{V}}_N(\Omega)$, $0 < t \le T$, such that

$$\begin{cases} (\partial_t \boldsymbol{w}_N, \boldsymbol{\phi}) + d(\nabla \boldsymbol{w}_N, \nabla \boldsymbol{\phi}) = (W(\boldsymbol{w}_N), \boldsymbol{\phi}) + (R(\boldsymbol{w}_N), \boldsymbol{\phi}), \\ \qquad\qquad \forall \boldsymbol{\phi} \in \boldsymbol{\mathcal{V}}_N(\Omega),\ 0 < t \le T, \\ \boldsymbol{w}_N(\boldsymbol{z},0) = \boldsymbol{w}_{N,0}(\boldsymbol{z}) = \boldsymbol{\Pi}_{N,\Omega} \boldsymbol{w}_0(\boldsymbol{z}), \quad \boldsymbol{z} \in \bar{\Omega}. \end{cases} \tag{3.3}$$

Next, we check the boundedness of solution of (3.3). To do this, we introduce quantities

$$\|\boldsymbol{w}\|^2_{\boldsymbol{\mathcal{H}}_d(\Omega)} = d_u |u|^2_{H^1(\Omega)} + d_v |v|^2_{H^1(\Omega)},$$
$$\mathcal{E}(\boldsymbol{w}, t) = \|\boldsymbol{w}(t)\|^2_{\mathbf{L}^2(\Omega)} + \int_0^t |\boldsymbol{w}(\xi)|^2_{\boldsymbol{\mathcal{H}}_d(\Omega)} d\xi. \tag{3.4}$$

Obviously, $\|\boldsymbol{w}\|_{\boldsymbol{\mathcal{H}}_d(\Omega)}$ and $\|\boldsymbol{w}\|_{\mathbf{H}^1(\Omega)}$ are equivalent, so we will not make a distinction.

Theorem 1. *Let* $\boldsymbol{w}_N(\boldsymbol{z},t) = \big(u_N(\boldsymbol{z},t), v_N(\boldsymbol{z},t)\big)^T$ *is solution of* (3.3). *Then, for any* $0 < t \le T$,

$$\mathcal{E}(\boldsymbol{w}_N, t) \le \rho_{N,0} e^{2t},$$

where $\rho_{N,0} = \|\boldsymbol{w}_{0,N}\|^2_{\boldsymbol{L}^2(\Omega)} + 2Ft$.

Proof. Set $\boldsymbol{\phi} = 2\boldsymbol{w}_N$ in (3.3), we have

$$(\partial_t \boldsymbol{w}_N, 2\boldsymbol{w}_N) + d(\nabla \boldsymbol{w}_N, 2\nabla \boldsymbol{w}_N) = (W(\boldsymbol{w}_N), 2\boldsymbol{w}_N) + (R(\boldsymbol{w}_N), 2\boldsymbol{w}_N). \quad (3.5)$$

By the Hölder inequality, we derive that

$$(W(\boldsymbol{w}_N), 2\boldsymbol{w}_N| \leq (4F + 2k)\|\boldsymbol{w}_N\|^2_{\mathbf{L}^2(\Omega)} + 2F. \quad (3.6)$$

Thanks to the Hölder inequality and the Young inequality with parameters $p = 4, q = \frac{4}{3}$, we deduce

$$\begin{aligned} |2(R(\boldsymbol{w}_N), \boldsymbol{w}_N)| &\leq \|u_N\|^4_{L^4(\Omega)} + \|v_N\|^4_{L^4(\Omega)} \\ &+ \frac{1}{2}\|u_N\|^4_{L^4(\Omega)} + \frac{3}{2}\|v_N\|^4_{L^4(\Omega)} \leq 3\|\boldsymbol{w}_N\|^4_{\mathbf{L}^4(\Omega)}. \end{aligned} \quad (3.7)$$

Substituting (3.6), (3.7) into (3.5) and using Poincaré inequality, the inverse inequality in Lemma 6 with $p = 2$, $q = 4$, we get

$$\partial_t \|\boldsymbol{w}_N\|^2_{\mathbf{L}^2(\Omega)} + |\boldsymbol{w}_N|^2_{\boldsymbol{\mathcal{H}}_d(\Omega)} \leq (2F + k)^2 \|\boldsymbol{w}_N\|^2_{\mathbf{L}^2(\Omega)} + 9N^2 \|\boldsymbol{w}_N\|^4_{\mathbf{L}^2(\Omega)} + 2F.$$

Then, we have

$$\partial_t \mathcal{E}(\boldsymbol{w}_N, t) \leq (2F + k)^2 \mathcal{E}(\boldsymbol{w}_N, t) + 9N^2 \mathcal{E}^2(\boldsymbol{w}_N, t) + 2F,$$

where $\mathcal{E}(\boldsymbol{w}_N, t)$ is defined in (3.4).
Integrating the above inequality on $[0, t]$ with respect to t, we yield

$$\mathcal{E}(\boldsymbol{w}_N, t) \leq \|\boldsymbol{w}_{N,0}\|^2_{\boldsymbol{L}^2} + 2Ft) + c\int_0^t (\mathcal{E}(\boldsymbol{w}_N, s) + N^2\mathcal{E}^2(\boldsymbol{w}_N, s))ds.$$

Let $\rho_{N,0} = \|\boldsymbol{w}_{0,N}\|^2_{\mathbf{L}^2(\Omega)} + 2Ft$. By Lemma 8, we have

$$E(\boldsymbol{w}_N, t) \leq \rho_{N,0} e^{2t}.$$

□

4 Error analysis

In this section, we analyze the stability and the convergence of the scheme (3.3). Because the system (3.3) is a nonlinear system, so we analyze its generalized stability. Let $\tilde{\boldsymbol{w}}_N(\boldsymbol{z})$ is the error of $\boldsymbol{w}_N(\boldsymbol{z})$ induced by the error $\tilde{\boldsymbol{w}}_{N,0}(\boldsymbol{z})$ of $\boldsymbol{w}_{N,0}(\boldsymbol{z})$. We obtain from (3.3) that

$$\begin{cases} (\partial_t \tilde{\boldsymbol{w}}_N, \boldsymbol{\phi}) + d(\nabla \tilde{\boldsymbol{w}}_N, \nabla \boldsymbol{\phi}) = (\tilde{W}(\tilde{\boldsymbol{w}}_N), \boldsymbol{\phi}) + (\tilde{R}(\tilde{\boldsymbol{w}}_N), \boldsymbol{\phi}), & \forall \boldsymbol{\phi} \in \boldsymbol{\mathcal{V}}_N(\Omega), \\ \tilde{\boldsymbol{w}}_{N,0}(\boldsymbol{z}) = \tilde{\boldsymbol{w}}_N(\boldsymbol{z}, 0), & \boldsymbol{z} \in \bar{\Omega}, \end{cases} \quad (4.1)$$

where

$$\tilde{W}(\tilde{\boldsymbol{w}}_N) = (-F\tilde{u}_N, -(F + k)\tilde{v}_N)^T, \qquad \tilde{R}(\tilde{\boldsymbol{w}}_N) = (R_1, R_2)^T,$$
$$R_1 = -(\tilde{u}_N\tilde{v}_N^2 + \tilde{u}_N v_N^2 + u_N\tilde{v}_N^2 + 2\tilde{u}_N v_N\tilde{v}_N + 2u_N v_N\tilde{v}_N), \qquad R_2 = -R_1.$$

Then, we have the following result of stability of the scheme (3.3).

Theorem 2. *Let $\boldsymbol{w}_N(\boldsymbol{z},t)$ is solution of (3.3). If $\boldsymbol{w}_{N,0}(\boldsymbol{z})$ has the error $\tilde{\boldsymbol{w}}_{N,0}(\boldsymbol{z})$. It induce the error of $\boldsymbol{w}_N(\boldsymbol{z},t)$ denoted by $\tilde{\boldsymbol{w}}_N(\boldsymbol{z},t)$. Suppose $\tilde{\rho}_{N,0}e^{2T} \leq N^{-2}$. Then, for any $0 < t \leq T$,*

$$\mathcal{E}(\tilde{\boldsymbol{w}}_N,t) \leq \tilde{\rho}_{N,0}e^{2t}, \quad \tilde{\rho}_{N,0} = \left\|\tilde{\boldsymbol{w}}_{N,0}\right\|^2_{\mathbf{L}^2(\Omega)}.$$

Proof. Choosing $\boldsymbol{\phi} = 2\tilde{\boldsymbol{w}}_N$ in (4.1), we get

$$\partial_t\|\tilde{\boldsymbol{w}}_N\|^2_{\mathbf{L}^2(\Omega)} + 2|\tilde{\boldsymbol{w}}_N|^2_{\boldsymbol{\mathcal{H}}_d(\Omega)} = 2\big(\tilde{W}(\tilde{\boldsymbol{w}}_N),\tilde{\boldsymbol{w}}_N\big) + 2\big(\tilde{R}(\tilde{\boldsymbol{w}}_N),\tilde{\boldsymbol{w}}_N\big). \tag{4.2}$$

Clearly,

$$\big|2(\tilde{W}\big(\tilde{\boldsymbol{w}}_N\big),\tilde{\boldsymbol{w}}_N)\big| \leq 2(F+k)\left\|\tilde{\boldsymbol{w}}_N\right\|^2_{\mathbf{L}^2(\Omega)}. \tag{4.3}$$

Next, we estimate $(\tilde{R}\big(\tilde{\boldsymbol{w}}_N\big),2\tilde{\boldsymbol{w}}_N)$. Obviously,

$$|2(\tilde{R}\big(\tilde{\boldsymbol{w}}_N\big),\tilde{\boldsymbol{w}}_N)| \leq 2|(R_1,\tilde{u}_N)| + 2|(R_2,\tilde{v}_N)|. \tag{4.4}$$

By Hölder inequality and Young inequality, we derive that

$$\big|2\left(R_1,\tilde{u}_N\right)\big| \leq 5\left\|\tilde{\boldsymbol{w}}_N\right\|^4_{\mathbf{L}^4(\Omega)} + 9\left\|\boldsymbol{w}_N\right\|^2_{\mathbf{L}^4(\Omega)}\left\|\tilde{\boldsymbol{w}}_N\right\|^2_{\mathbf{L}^4(\Omega)}, \tag{4.5}$$

$$\big|2\left(R_2,\tilde{v}_N\right)\big| \leq 5\|\tilde{\boldsymbol{w}}_N\|^4_{\mathbf{L}^4(\Omega)} + 9\|\boldsymbol{w}_N\|^2_{\mathbf{L}^4(\Omega)}\|\tilde{\boldsymbol{w}}_N\|^2_{\mathbf{L}^4(\Omega)}. \tag{4.6}$$

Substituting (4.5), (4.6) into (4.4), and using Lemmas 6 and 7, we check that

$$\big|2\big(\tilde{R}(\tilde{\boldsymbol{w}}_N),\tilde{\boldsymbol{w}}_N\big)\big| \leq 30N^2\left\|\tilde{\boldsymbol{w}}_N\right\|^4_{\mathbf{L}^2(\Omega)} + c\left\|\boldsymbol{w}_N\right\|_{\mathbf{L}^2(\Omega)}\left\|\boldsymbol{w}_N\right\|_{\mathbf{H}^1(\Omega)}\left\|\tilde{\boldsymbol{w}}_N\right\|^2_{\mathbf{L}^2(\Omega)}. \tag{4.7}$$

Combining (4.3), (4.7) with (4.2), and using the Poincaré inequality lead to

$$\partial_t\left\|\tilde{\boldsymbol{w}}_N\right\|^2_{\mathbf{L}^2(\Omega)} + |\tilde{\boldsymbol{w}}_N|^2_{\boldsymbol{\mathcal{H}}_d(\Omega)} \leq \rho(\boldsymbol{w}_N)\left\|\tilde{\boldsymbol{w}}_N\right\|^2_{\mathbf{L}^2(\Omega)} + 30N^2\left\|\tilde{\boldsymbol{w}}_N\right\|^4_{\mathbf{L}^2(\Omega)},$$

where $\rho(\boldsymbol{w}_N) = ((F+k)^2 + \|\boldsymbol{w}_N\|_{\mathbf{L}^2(\Omega)}\|\boldsymbol{w}_N\|_{\mathbf{H}^1(\Omega)})$ is positive and bounded. Furthermore, from the above inequality we have

$$\partial_t\mathcal{E}(\tilde{\boldsymbol{w}}_N,t) \leq \hat{\rho}(\boldsymbol{w}_N)(\mathcal{E}(\tilde{\boldsymbol{w}}_N,t) + N^2\mathcal{E}^2(\tilde{\boldsymbol{w}}_N,t)), \tag{4.8}$$

where $\hat{\rho}(\boldsymbol{w}_N) = \rho(\boldsymbol{w}_N) + 30$. Integrating (4.8) on $[0,t]$, we yield

$$\mathcal{E}(\tilde{\boldsymbol{w}}_N,t) \leq \|\tilde{\boldsymbol{w}}_{N,0}\|^2_{\mathbf{L}^2(\Omega)} + \hat{\rho}(\boldsymbol{w}_N)\int_0^t(\mathcal{E}(\tilde{\boldsymbol{w}}_N,s) + N^2\mathcal{E}^2(\tilde{\boldsymbol{w}}_N,s))ds.$$

Let $\tilde{\rho}_{N,0} = \left\|\tilde{\boldsymbol{w}}_{N,0}\right\|^2_{\mathbf{L}^2(\Omega)}$. By Lemma 8, we get

$$\mathcal{E}(\tilde{\boldsymbol{w}}_N,t) \leq \tilde{\rho}_{N,0}e^{2t}.$$

□

Now, we are position to discuss convergence of scheme (3.3).

Theorem 3. *Let $\boldsymbol{w}(\boldsymbol{z})$ and $\boldsymbol{w}_N(\boldsymbol{z})$ are the solutions of (3.2) and (3.3) respectively. If $N \geq 4$, $2 \leq r \leq N+1$, $\boldsymbol{w} \in H^1(0,T;\boldsymbol{\mathcal{V}}(\Omega)) \cap L^\infty(0,T;\boldsymbol{\mathcal{H}}_d(\Omega))$, and exists $T>0$ such that,*

$$\tilde{\rho}_0 e^{2T} N^{2-2r} \leq N^{-2},$$

Then, for any $0 \leq t \leq T$,

$$\mathcal{E}(\boldsymbol{w}_N - \boldsymbol{w}, t) \leq c N^{2-2r} \rho_0,$$

where c is a positive constant independent of r, N, $\boldsymbol{w}$, and $\rho_0 = e^{2t}\big(A_r^2(\boldsymbol{w}_0) + B_r^2(\boldsymbol{w}_0) + \int_0^t (B_r^2(\boldsymbol{w}) + B_r^2(\partial_t \boldsymbol{w}) + B_r^4(\boldsymbol{w}))d\xi\big) + B_r^2(\boldsymbol{w}) + \int_0^t B_r^2(\boldsymbol{w})d\xi$.

Proof. Let $\mathbf{V}_N^* = \boldsymbol{\Pi}_{N,\Omega}^{1,0}\boldsymbol{w} = (U_N^*, V_N^*)^T$ and $\tilde{\mathbf{V}}_N = \boldsymbol{w}_N - \mathbf{V}_N^*$. Denote $\boldsymbol{f} = \big(-F(u-U_N^*), -(F+k)(v-V_N^*)\big)^T$, $\boldsymbol{g} = (-g_1, g_1)^T$, where

$$\begin{aligned} g_1 =& (u-U_N^*)(v-V_N^*)^2 + (u-U_N^*)(V_N^*)^2 + U_N^*(v-V_N^*)^2 \\ &+ 2(u-U_N^*)(v-V_N^*)V_N^* + 2U_N^*(v-V_N^*)V_N^*. \end{aligned}$$

We get from (3.2) that

$$\begin{cases} (\partial_t \mathbf{V}_N^*, \boldsymbol{\phi}) + d\,(\nabla \mathbf{V}_N^*, \nabla \boldsymbol{\phi}) \\ \quad = \big(W(\mathbf{V}_N^*), \boldsymbol{\phi}\big) + \big(R(\mathbf{V}_N^*), \boldsymbol{\phi}\big) + \sum_{l=1}^{4} G_l(\boldsymbol{\phi}, t), \quad \forall \boldsymbol{\phi} \in \boldsymbol{\mathcal{V}}_N(\Omega), \\ \mathbf{V}_N^*(0) = \boldsymbol{\Pi}_{N,\Omega}^{1,0}\boldsymbol{w}_0, \end{cases} \tag{4.9}$$

where

$$\begin{aligned} &G_1(\boldsymbol{\phi}, t) = -(\partial_t(\boldsymbol{w} - \mathbf{V}_N^*), \boldsymbol{\phi}), \quad G_2(\boldsymbol{\phi}, t) = -d(\nabla(\boldsymbol{w} - \mathbf{V}_N^*), \nabla\boldsymbol{\phi}), \\ &G_3(\boldsymbol{\phi}, t) = (\boldsymbol{f}, \boldsymbol{\phi}), \qquad\qquad G_4(\boldsymbol{\phi}, t) = (\boldsymbol{g}, \boldsymbol{\phi}). \end{aligned}$$

Subtracting (4.9) from (3.3) and choose $\phi = 2\tilde{\mathbf{V}}_N$, we get

$$\begin{aligned} &\partial_t \|\tilde{\mathbf{V}}_N\|_{\mathbf{L}^2(\Omega)}^2 + 2|\tilde{\mathbf{V}}_N|_{\boldsymbol{\mathcal{H}}_d(\Omega)}^2 = 2\big(W(\boldsymbol{w}_N) - W(\mathbf{V}_N^*), \tilde{\mathbf{V}}_N\big) \\ &\quad + 2\big(R(\boldsymbol{w}_N) - R(\mathbf{V}_N^*), \tilde{\mathbf{V}}_N\big) - 2\sum_{l=1}^{4} G_l(\tilde{\mathbf{V}}_N, t), \\ &\tilde{\mathbf{V}}_{N,0} = \boldsymbol{\Pi}_{N,\Omega}\boldsymbol{w}_0 - \boldsymbol{\Pi}_{N,\Omega}^{1,0}\boldsymbol{w}_0. \end{aligned} \tag{4.10}$$

Using the Hölder inequality, we derive that

$$2\big|\big(W(\boldsymbol{w}_N) - W(\mathbf{V}_N^*), \tilde{\mathbf{V}}_N\big)\big| \leq 4(F+k)\big\|\tilde{\mathbf{V}}_N\big\|_{\mathbf{L}^2(\Omega)}^2, \tag{4.11}$$

$$2\big|\big(R(\boldsymbol{w}_N) - R(\mathbf{V}_N^*), \tilde{\mathbf{V}}_N\big)\big| \leq 2\big|(r_1, \tilde{U}_N)\big| + 2\big|(-r_1, \tilde{V}_N)\big|, \tag{4.12}$$

where

$$r_1 = -\big(\tilde{U}_N\tilde{V}_N^2 + \tilde{U}_N {V_N^*}^2 + U_N^*\tilde{V}_N^2 + 2\tilde{U}_N\tilde{V}_N V_N^* + 2U_N^*\tilde{V}_N V_N^*\big).$$

Thanks to the Hölder inequality, (2.10), the Poincaré inequality, the Young inequality and Lemma 5 with $r = 1$, we yield that

$$2\Big|\Big(r_1, \tilde{U}_N\Big)\Big| \leq 5\big\|\tilde{\mathbf{V}}_N\big\|^4_{\mathbf{L}^4(\Omega)} + cB_1^2(\boldsymbol{w})\big\|\tilde{\mathbf{V}}_N\big\|^2_{\boldsymbol{\mathcal{H}}_d(\Omega)}, \tag{4.13}$$

$$2|(-r_1, \tilde{V}_N)| \leq 5\big\|\tilde{\mathbf{V}}_N\big\|^4_{\mathbf{L}^4(\Omega)} + cB_1^2(\boldsymbol{w})\big\|\tilde{\mathbf{V}}_N\big\|^2_{\boldsymbol{\mathcal{H}}_d(\Omega)}. \tag{4.14}$$

Substituting (4.13), (4.14) into (4.12), and using Lemma 6 with $p = 2$, $q = 4$ leads to

$$2|(R(\boldsymbol{w}_N) - R(\mathbf{V}_N^*), \tilde{\mathbf{V}}_N)| \leq 30N^2\|\tilde{\mathbf{V}}_N\|^4_{\mathbf{L}^2(\Omega)} + cB_1^2(\boldsymbol{w})\|\tilde{\mathbf{V}}_N\|^2_{\boldsymbol{\mathcal{H}}_d(\Omega)}. \tag{4.15}$$

Next, we estimate $2G_j(\tilde{\mathbf{V}}_N, t),\ j = 1, \ldots, 4$. Employing the Hölder inequality, Lemma 5 and the Poincaré inequality, we deduce

$$2|G_1(\tilde{\mathbf{V}}_N, t)| \leq cN^{2-2r}B_r^2\left(\partial_t \boldsymbol{w}\right) + \big\|\tilde{\mathbf{V}}_N\big\|^2_{\mathbf{L}^2(\Omega)}, \tag{4.16}$$

$$2|G_2(\tilde{\mathbf{V}}_N, t)| \leq cN^{2-2r}B_r^2\big(\boldsymbol{w}\big) + \big|\tilde{\mathbf{V}}_N\big|^2_{\boldsymbol{\mathcal{H}}_d(\Omega)}, \tag{4.17}$$

$$2|G_3(\tilde{\mathbf{V}}_N, t)| \leq cN^{2-2r}B_r^2(\boldsymbol{w}) + (F+k)\big\|\tilde{\mathbf{V}}_N\big\|^2_{\mathbf{L}^2(\Omega)}, \tag{4.18}$$

$$2|G_4(\tilde{\mathbf{V}}_N, t)| \leq 2|(g_1, \tilde{U}_N)| + 2|(g_1, \tilde{V}_N)|. \tag{4.19}$$

By the Hölder inequality, we have that

$$\begin{aligned} 2\big|\big(g_1, \tilde{U}_N\big)\big| \leq{}& \frac{9}{2}\big\|\boldsymbol{w}-\mathbf{V}_N^*\big\|^4_{\mathbf{L}^4(\Omega)} + 3\big\|\boldsymbol{w}-\mathbf{V}_N^*\big\|^2_{\mathbf{L}^4(\Omega)} + \frac{1}{2}\big\|\tilde{\mathbf{V}}_N\big\|^4_{\mathbf{L}^4(\Omega)} \\ &+ 3\big\|\mathbf{V}_N^*\big\|^2_{\mathbf{L}^4(\Omega)}\big\|\tilde{\mathbf{V}}_N\big\|^2_{\mathbf{L}^4(\Omega)} + 3\big\|\mathbf{V}_N^*\big\|^4_{\mathbf{L}^4(\Omega)}\big\|\tilde{\mathbf{V}}_N\big\|^2_{\mathbf{L}^4(\Omega)}, \end{aligned} \tag{4.20}$$

$$\begin{aligned} 2\big|\big(-g_1, \tilde{V}_N\big)\big| \leq{}& \frac{9}{2}\big\|\boldsymbol{w} - \mathbf{V}_N^*\big\|^4_{\mathbf{L}^4(\Omega)} + 3\big\|\boldsymbol{w} - \mathbf{V}_N^*\big\|^2_{\mathbf{L}^4(\Omega)} + \frac{1}{2}\big\|\tilde{\mathbf{V}}_N\big\|^4_{\mathbf{L}^4(\Omega)} \\ &+ 3\big\|\mathbf{V}_N^*\big\|^2_{\mathbf{L}^4(\Omega)}\big\|\tilde{\mathbf{V}}_N\big\|^2_{\mathbf{L}^4(\Omega)} + 3\big\|\mathbf{V}_N^*\big\|^4_{\mathbf{L}^4(\Omega)}\big\|\tilde{\mathbf{V}}_N\big\|^2_{\mathbf{L}^4(\Omega)}. \end{aligned} \tag{4.21}$$

Substituting (4.20), (4.21) into (4.19), and using Lemma 7, Lemma 6, the Poincaré inequality and Lemma 5, we check that

$$\begin{aligned} 2\big|G_4(\tilde{\mathbf{V}}_N, t)\big| \leq{}& cN^{4-4r}B_r^4(\boldsymbol{w}) + cN^{2-2r}B_r^2(\boldsymbol{w}) + 9N^2\big\|\tilde{\mathbf{V}}_N\big\|^4_{\mathbf{L}^2(\Omega)} \\ &+ cB_1^2(\boldsymbol{w})\big|\tilde{\mathbf{V}}_N\big|^2_{\boldsymbol{\mathcal{H}}_d(\Omega)} + cB_1^4(\boldsymbol{w})\big|\tilde{\mathbf{V}}_N\big|^2_{\boldsymbol{\mathcal{H}}_d(\Omega)}. \end{aligned} \tag{4.22}$$

Inserting (4.11), (4.15)–(4.18), (4.22) into (4.10), we have

$$\begin{aligned} &\partial_t\big\|\tilde{\mathbf{V}}_N\big\|^2_{\mathbf{L}^2(\Omega)} + \big|\tilde{\mathbf{V}}_N\big|^2_{\boldsymbol{\mathcal{H}}_d(\Omega)} \\ &\leq cN^{2-2r}\tilde{\tilde{\rho}}_0(\boldsymbol{w}) + \tilde{\eta}(\boldsymbol{w})\big(\big\|\tilde{\mathbf{V}}_N\big\|^2_{\mathbf{L}^2(\Omega)} + \big|\tilde{\mathbf{V}}_N\big|^2_{\boldsymbol{\mathcal{H}}_d(\Omega)} + N^2\big\|\tilde{\mathbf{V}}_N\big\|^4_{\mathbf{L}^2(\Omega)}\big), \end{aligned} \tag{4.23}$$

where

$$\begin{aligned} \tilde{\tilde{\rho}}_0(\boldsymbol{w}) &= B_r^2\left(\boldsymbol{w}\right) + B_r^2\left(\partial_t \boldsymbol{w}\right) + B_r^4(\boldsymbol{w}), \\ \tilde{\eta}(\boldsymbol{w}) &= 40 + 5(F+k) + B_1^2(\boldsymbol{w}) + B_1^4(\boldsymbol{w}). \end{aligned}$$

Let $\mathcal{E}(\tilde{\mathbf{V}}_N,t)$ be the same as in (3.4). Clearly, (4.23) can be written as

$$\partial_t\mathcal{E}(\tilde{\mathbf{V}}_N,t)\le cN^{2-2r}\tilde{\tilde{\rho}}_0(\boldsymbol{w})+\tilde{\eta}(\boldsymbol{w})\left(\mathcal{E}(\tilde{\mathbf{V}}_N,t)+N^2\mathcal{E}^2(\tilde{\mathbf{V}}_N,t)\right).$$

Integrating the above inequality on $[0,t]$ with respect to t, we get

$$\begin{aligned}\mathcal{E}(\tilde{\mathbf{V}}_N,t)\le&\mathcal{E}(\tilde{\mathbf{V}}_N,0)+cN^{2-2r}\int_0^t\tilde{\tilde{\rho}}_0(\boldsymbol{w})d\xi\\&+\eta(\boldsymbol{w})\int_0^t(\mathcal{E}(\tilde{\mathbf{V}}_N,\xi)+N^2\mathcal{E}^2(\tilde{\mathbf{V}}_N,\xi))d\xi,\end{aligned}\tag{4.24}$$

where $\eta(\boldsymbol{w})=\max\limits_{\xi\in[0,t]}\tilde{\eta}(\boldsymbol{w}(\xi))$. According to $\boldsymbol{\xi}_{xy}^{-2}>1$, Lemmas 4 and 5, we check that

$$\left\|\tilde{\mathbf{V}}_{N,0}\right\|^2_{\mathbf{L}^2(\Omega)}\le cN^{2-2r}\big(A_r^2(\boldsymbol{w}_0)+B_r^2(\boldsymbol{w}_0)\big).\tag{4.25}$$

Combining (4.24) with (4.25) leads to

$$\mathcal{E}(\tilde{\mathbf{V}}_N,t)\le cN^{2-2r}\tilde{\rho}_0(\boldsymbol{w})+\eta(\boldsymbol{w})\int_0^t\big(\mathcal{E}(\tilde{\mathbf{V}}_N,\xi)+N^2\mathcal{E}^2(\tilde{\mathbf{V}}_N,\xi)\big)d\xi,\tag{4.26}$$

where

$$\tilde{\rho}_0=A_r^2(\boldsymbol{w}_0)+B_r^2(\boldsymbol{w}_0)+\int_0^t\tilde{\tilde{\rho}}_0(\boldsymbol{w})d\xi.$$

According to Lemma 8 with $\rho=cN^{2-2r}\tilde{\rho}_0(\boldsymbol{w})$, $n=2$ and $d_k=2$, we have

$$\mathcal{E}(\tilde{\mathbf{V}}_N,t)\le cN^{2-2r}\tilde{\rho}_0e^{2t}.$$

Employing Lemma 5, we deduce that

$$\mathcal{E}(\mathbf{V}_N^*-\boldsymbol{w},t)\le cN^{2-2r}(B_r^2(\boldsymbol{w})+\int_0^tB_r^2(\boldsymbol{w})d\xi).\tag{4.27}$$

Setting

$$\rho_0=\tilde{\rho}_0e^{2t}+B_r^2(\boldsymbol{w})+\int_0^tB_r^2(\boldsymbol{w})d\xi.$$

Thanks to (4.26) and (4.27), we derive that

$$\mathcal{E}(\boldsymbol{w}_N-\boldsymbol{w},t)\le\mathcal{E}(\boldsymbol{w}_N-\mathbf{V}_N^*,t)+\mathcal{E}(\mathbf{V}_N^*-\boldsymbol{w},t)\le cN^{2-2r}\rho_0.$$

□

Remark 1. According to Lemma 8, the stability and convergence results require the conditions $\tilde{\rho}_{N,0}e^{2T}\le N^{-2}$ and $\tilde{\rho}_0e^{2T}N^{2-2r}\le N^{-2}$, respectively. These imply small-data or short-time conditions necessary. We emphasize that these restrictions arise from the proof technique rather than from any fundamental limitation of the numerical scheme itself. Indeed, the numerical experiments, particularly the long-time simulation in Figures 3 and 5 indicate that the method remains stable in practice well beyond these theoretical constraints.

5 Numerical results

In this section, we will provide a detailed description of the numerical implementation and present the corresponding numerical results. Let $\{x_m, \alpha_m\}_{m=0}^{N}$, $\{y_n, \beta_n\}_{n=0}^{N}$ denote the Legendre-Gauss nodes and weights in the x-direction and y-direction, respectively.
The numerical solution $\boldsymbol{w}_N(\boldsymbol{z},t) = (u_N(\boldsymbol{z},t), v_N(\boldsymbol{z},t))^T$ can be expanded as

$$\begin{aligned}\boldsymbol{w}_N(\boldsymbol{z},t) &= (u_N(\boldsymbol{z},t),\ v_N(\boldsymbol{z},t))^T \\ &= \Big(\sum_{l_1=4}^{N}\sum_{l_2=4}^{N}\hat{u}_{l_1,l_2}(t)\phi_{l_1,l_2}(\boldsymbol{z}),\ \sum_{l_1=4}^{N}\sum_{l_2=4}^{N}\hat{v}_{l_1,l_2}(t)\phi_{l_1,l_2}(\boldsymbol{z})\Big)^T.\end{aligned} \tag{5.1}$$

Substituting (5.1) into (3.3) and choosing $\boldsymbol{\phi} = \boldsymbol{\phi}_{k_1,k_2}(\boldsymbol{z})$, we get

$$\begin{cases}\displaystyle\sum_{l_1=4}^{N}\sum_{l_2=4}^{N}a_{k_1,k_2,l_1,l_2}\partial_t\hat{u}_{l_1,l_2}(t) + d_u\sum_{l_1=4}^{N}\sum_{l_2=4}^{N}b_{k_1,k_2,l_1,l_2}\hat{u}_{l_1,l_2}(t) \\ \displaystyle + F\sum_{l_1=4}^{N}\sum_{l_2=4}^{N}a_{k_1,k_2,l_1,l_2}\hat{u}_{l_1,l_2}(t) + f_{k_1,k_2} + q_{k_1,k_2}(t) = 0,\ 4\le k_1,k_2\le N, \\ \displaystyle\sum_{l_1=4}^{N}\sum_{l_2=4}^{N}a_{k_1,k_2,l_1,l_2}\partial_t\hat{v}_{l_1,l_2}(t) + d_v\sum_{l_1=4}^{N}\sum_{l_2=4}^{N}b_{k_1,k_2,l_1,l_2}\hat{v}_{l_1,l_2}(t) \\ \displaystyle + (F+k)\sum_{l_1=4}^{N}\sum_{l_2=4}^{N}a_{k_1,k_2,l_1,l_2}\hat{v}_{l_1,l_2}(t) - q_{k_1,k_2}(t) = 0,\ 4\le k_1,k_2\le N,\end{cases} \tag{5.2}$$

where

$$a_{k_1,k_2,l_1,l_2} = \int_{-1}^{1}\int_{-1}^{1}\psi_{l_1}(x)\psi_{l_2}(y)\psi_{k_1}(x)\psi_{k_2}(y)dxdy, \tag{5.3}$$

$$\begin{aligned}b_{k_1,k_2,l_1,l_2} = \int_{-1}^{1}\int_{-1}^{1}\Big(&\partial_x\psi_{l_1}(x)\psi_{l_2}(y)\partial_x\psi_{k_1}(x)\psi_{k_2}(y) \\ &+ \psi_{l_1}(x)\partial_y\psi_{l_2}(y)\psi_{k_1}(x)\partial_y\psi_{k_2}(y)\Big)dxdy,\end{aligned} \tag{5.4}$$

$$\begin{aligned}f_{k_1,k_2} &= \big(-F,\phi_{k_1,k_2}(\boldsymbol{z})\big) \approx -F\sum_{m=0}^{N}\sum_{n=0}^{N}\psi_{k_1}(x_m)\psi_{k_2}(y_n)\alpha_m\beta_n, q_{k_1,k_2}(t) \\ &= \Big(u_N(\boldsymbol{z},t)v_N^2(\boldsymbol{z},t),\phi_{k_1,k_2}(\boldsymbol{z})\Big) \approx \Big\langle u_N(\boldsymbol{z},t)v_N^2(\boldsymbol{z},t),\phi_{k_1,k_2}(\boldsymbol{z})\Big\rangle_N \\ &= \sum_{m=0}^{N}\sum_{n=0}^{N}u_N(x_m,y_n,t)v_N^2(x_m,y_n,t)\psi_{k_1}(x_m)\psi_{k_2}(y_n)\alpha_m\beta_n.\end{aligned}$$

For notational convenient, we denote

$$\xi_\lambda = \frac{2}{2\lambda+1},\quad \eta_{\lambda,\mu} = \int_{I_z}\psi_\lambda(z)\psi_\mu(z)dz,\quad \zeta_{\lambda,\mu} = \int_{I_z}\partial_z\psi_\lambda(z)\partial_z\psi_\mu(z)dz.$$

According to (2.2), (2.3) and (2.1) with $\alpha = \beta = 0$, we derive that

$$\eta_{\lambda,\mu} = \begin{cases} \xi_{\lambda-2}\xi_{\lambda-1}\xi_{\lambda}\xi_{\lambda+1}\xi_{\lambda+2}, & \mu = \lambda+4, \\ -2\xi_{\lambda-2}\xi_{\lambda-1}^2\xi_{\lambda}\left(\xi_{\lambda-3}+\xi_{\lambda+1}\right), & \mu = \lambda+2, \\ \xi_{\lambda-2}(\xi_{\lambda-4}\xi_{\lambda-3}^2\xi_{\lambda-2} + 4\xi_{\lambda-3}^2\xi_{\lambda-1}^2 + \xi_{\lambda-2}\xi_{\lambda-1}^2\xi_{\lambda}), & \mu = \lambda, \\ -2\xi_{\lambda-4}\xi_{\lambda-3}^2\xi_{\lambda-2}\left(\xi_{\lambda-5}+\xi_{\lambda-1}\right), & \mu = \lambda-2, \\ \xi_{\lambda-6}\xi_{\lambda-5}\xi_{\lambda-4}\xi_{\lambda-3}\xi_{\lambda-2}, & \mu = \lambda-4, \\ 0, & \text{otherwise.} \end{cases}$$

$$\zeta_{\lambda,\mu} = \begin{cases} -4\xi_{\lambda-2}\xi_{\lambda-1}\xi_{\lambda}, & \mu = \lambda+2, \\ 4\xi_{\lambda-2}^2\left(\xi_{\lambda-3}+\xi_{\lambda-1}\right), & \mu = \lambda, \\ -4\xi_{\lambda-4}\xi_{\lambda-3}\xi_{\lambda-2}, & \mu = \lambda-2, \\ 0, & \text{otherwise.} \end{cases}$$

Let $\mathcal{M} = (\eta_{\lambda,\mu})_{4\le\lambda,\mu\le N}$, $\mathcal{S} = (\zeta_{\lambda,\mu})_{4\le\lambda,\mu\le N}$. Furthermore, we denote $\mathcal{C} = (f_{k_1,k_2})_{4\le k_1,k_2\le N}$, $\mathcal{Q}(t) = (q_{k_1,k_2}(t))_{4\le k_1,k_2\le N}$, and

$$\mathcal{U}(t) = \begin{bmatrix} \hat{u}_{4,4}(t) & \cdots & \hat{u}_{4,N}(t) \\ \hat{u}_{5,4}(t) & \cdots & \hat{u}_{5,N}(t) \\ \vdots & & \vdots \\ \hat{u}_{N,4}(t) & \cdots & \hat{u}_{N,N}(t) \end{bmatrix}, \quad \mathcal{V}(t) = \begin{bmatrix} \hat{v}_{4,4}(t) & \cdots & \hat{v}_{4,N}(t) \\ \hat{v}_{5,4}(t) & \cdots & \hat{v}_{5,N}(t) \\ \vdots & & \vdots \\ \hat{v}_{N,4}(t) & \cdots & \hat{v}_{N,N}(t) \end{bmatrix}.$$

Then, the system (5.2) can written as

$$\begin{cases} \mathcal{M}\partial_t\mathcal{U}(t)\mathcal{M}^T + d_u(\mathcal{M}\mathcal{U}(t)\mathcal{S}^T + \mathcal{S}\mathcal{U}(t)\mathcal{M}^T) \\ \qquad\qquad + F\mathcal{M}\mathcal{U}(t)\mathcal{M}^T + \mathcal{C} + \mathcal{Q}(t) = 0, \\ \mathcal{M}\partial_t\mathcal{V}(t)\mathcal{M}^T + d_v(\mathcal{M}\mathcal{V}(t)\mathcal{S}^T + \mathcal{S}\mathcal{V}(t)\mathcal{M}^T) \\ \qquad\qquad + (F+k)\mathcal{M}\mathcal{U}(t)\mathcal{M}^T - \mathcal{Q}(t) = 0. \end{cases} \tag{5.5}$$

Denote,

$$\begin{aligned} A =& (a_{k_1,k_2,l_1,l_2})_{4\le k_1,k_2,l_1,l_2\le N}, \quad B = (b_{k_1,k_2,l_1,l_2})_{4\le k_1,k_2,l_1,l_2\le N}, \\ \hat{U}(t) =& (\hat{u}_{4,4}(t), \hat{u}_{4,5}(t), \cdots, \hat{u}_{4,N}(t), \cdots, \hat{u}_{N,4}(t), \hat{u}_{N,5}(t), \cdots, \hat{u}_{N,N}(t))^T, \\ \hat{V}(t) =& (\hat{v}_{4,4}(t), \hat{v}_{4,5}(t), \cdots, \hat{v}_{4,N}(t), \cdots, \hat{v}_{N,4}(t), \hat{v}_{N,5}(t), \cdots, \hat{v}_{N,N}(t))^T, \\ \hat{C} =& (f_{4,4}, f_{4,5}, \cdots, f_{4,N}, \cdots, f_{N,4}, f_{N,5}, \cdots, f_{N,N})^T, \\ \hat{Q}(t) =& (q_{4,4}(t), q_{4,5}(t), \cdots, q_{4,N}(t), \cdots, q_{N,4}(t), q_{N,5}(t), \cdots, q_{N,N}(t))^T. \end{aligned}$$

Equations (5.3) and (5.4) indicate

$$A = \mathcal{M} \otimes \mathcal{M}, \qquad B = \mathcal{S} \otimes \mathcal{M} + \mathcal{M} \otimes \mathcal{S}.$$

Then, (5.5) can be written as

$$\begin{cases} A\partial_t\hat{U}(t) + d_u B\hat{U}(t) + FA\hat{U}(t) + \hat{C} + \hat{Q}(t) = 0, \\ A\partial_t\hat{V}(t) + d_v B\hat{V}(t) + (F+k)A\hat{V}(t) - \hat{Q}(t) = 0. \end{cases} \tag{5.6}$$

Moreover, let

$$\hat{\boldsymbol{U}}(t)=(\hat{U}(t),\hat{V}(t))^T,\quad \boldsymbol{A}=\begin{bmatrix}A & \\ & A\end{bmatrix},\quad \boldsymbol{B}=\begin{bmatrix}d_uB & \\ & d_vB\end{bmatrix},$$
$$\boldsymbol{D}=\begin{bmatrix}FA & \\ & (F+k)A\end{bmatrix},\quad \boldsymbol{C}=\left(\hat{C},\boldsymbol{0}\right)^T,\boldsymbol{Q}(t)=\left(\hat{Q}(t),-\hat{Q}(t)\right)^T.$$

System (5.6) can be written in the following compact form

$$\boldsymbol{A}\partial_t\hat{\boldsymbol{U}}(t)+\boldsymbol{B}\hat{\boldsymbol{U}}(t)+\boldsymbol{D}\hat{\boldsymbol{U}}(t)+\boldsymbol{C}+\boldsymbol{Q}(t)=\boldsymbol{0}. \tag{5.7}$$

Remark 2. The matrix $\mathcal{M}$ is nine-diagonal, while $\mathcal{S}$ is penta-diagonal. Consequently, the matrices $\mathbf{A}$, $\mathbf{B}$, and $\mathbf{D}$ are sparse, which improves the conditioning of the system (5.7). As a result, the disrete system can be inverted efficiently.

To calculate the numerical error, we introduce a source term $\breve{\mathbf{g}}(\boldsymbol{z},t)=(g_u(\boldsymbol{z},t),$ $g_v(\boldsymbol{z},t))^T$ on the right-hand side of (3.1). Denote

$$\begin{aligned}G_u(t)=&(\hat{g}_{4,4}(t),\hat{g}_{4,5}(t),\cdots,\hat{g}_{4,N}(t),\cdots,\hat{g}_{N,4}(t),\hat{g}_{N,5}(t),\cdots,\hat{g}_{N,N}(t))^T,\\ G_v(t)=&(\tilde{g}_{4,4}(t),\tilde{g}_{4,5}(t),\cdots,\tilde{g}_{4,N}(t),\cdots,\tilde{g}_{N,4}(t),\tilde{g}_{N,5}(t),\cdots,\tilde{g}_{N,N}(t))^T\end{aligned}$$

with

$$\begin{aligned}\hat{g}_{k_1,k_2}(t)=&(g_u(\boldsymbol{z},t),\phi_{k_1,k_2}(\boldsymbol{z}))\approx\sum_{m=0}^{N}\sum_{n=0}^{N}g_u(x_m,y_n,t)\psi_{k_1}(x_m)\psi_{k_2}(y_n)\alpha_m\beta_n,\\ \tilde{g}_{k_1,k_2}(t)=&(g_v(\boldsymbol{z},t),\phi_{k_1,k_2}(\boldsymbol{z}))\approx\sum_{m=0}^{N}\sum_{n=0}^{N}g_v(x_m,y_n,t)\psi_{k_1}(x_m)\psi_{k_2}(y_n)\alpha_m\beta_n.\end{aligned}$$

Then, we get

$$\boldsymbol{A}\partial_t\hat{\boldsymbol{U}}(t)+\boldsymbol{B}\hat{\boldsymbol{U}}(t)+\boldsymbol{D}\hat{\boldsymbol{U}}(t)+\boldsymbol{C}+\boldsymbol{Q}(t)=\boldsymbol{G}(t), \tag{5.8}$$

where $\boldsymbol{G}(t)=(G_u(t),G_v(t))^T$.

We use the BDF2 scheme with time step τ to discrete the above system (5.8) in time as:

$$\begin{aligned}\boldsymbol{A}\frac{3\hat{\mathbf{U}}(t_{n+1})-4\hat{\mathbf{U}}(t_n)+\hat{\mathbf{U}}(t_{n-1})}{2\tau}+\boldsymbol{B}\hat{\mathbf{U}}(t_{n+1})+\boldsymbol{D}\hat{\mathbf{U}}(t_{n+1})\\ +\boldsymbol{C}(t_{n+1})+\boldsymbol{Q}(t_{n+1})=\boldsymbol{G}(t_{n+1}),\quad 1\le n\le Q-1,\end{aligned} \tag{5.9}$$

where $t_n=n\tau$ and Q is a positive integer. We obtain the following result for the temporal convergence.

Theorem 4. *Let the time step size be τ and $t_n = n\tau$. Assume that the exact solution $\hat{\mathbf{U}}(t)$ satisfies $\hat{\mathbf{U}}_{ttt} \in L^\infty(0,T;L^2(\Omega))$. Then the local truncation error satisfies*

$$\left\| \boldsymbol{A}\Big(\frac{3\hat{\mathbf{U}}(t_{n+1}) - 4\hat{\mathbf{U}}(t_n) + \hat{\mathbf{U}}(t_{n-1})}{2\tau} - \hat{\mathbf{U}}_t(t_{n+1})\Big)\right\| \le C_A\tau^2, \tag{5.10}$$

where $C_A = C\,\|\boldsymbol{A}\|\,\|\widehat{\mathbf{U}}_{ttt}\|_{L^\infty(0,T;L^2(\Omega))}$ and $\|\boldsymbol{A}\|$ denotes the norm of $\boldsymbol{A}$.

Proof. The result (5.10) can be derived easily by using Taylor expansions with integral remainders. □

We use the following $L^\infty-$norm to describe the numerical error:

$$E_{N,\tau}(t) = \max_{0\le m\le N}\max_{0\le n\le N}\{\ |\boldsymbol{w}(x_m,y_n,t) - \boldsymbol{w}_{N,\tau}(x_m,y_n,t)|\ \}.$$

Example 1. We choose the test function:

$$\begin{cases} u(x,y,t) = \cos(t)\,(1-x^2)\,(1-y^2)\,\sin(4\pi x)\,\sin(4\pi y), \\ v(x,y,t) = \cos(t)\,(1-x^2)\,(1-y^2)\,\sin(4\pi x)\,\sin(4\pi y). \end{cases} \tag{5.11}$$

Table 1. Temporal convergence test with test function (5.11).

τ	$E_{N,\tau}$	Order
1/8	1.1732E-05	-
1/16	3.0883E-06	1.93
1/32	7.8266E-07	1.98
1/64	1.9492E-07	2.01
1/128	4.6613E-08	2.06

In Table 1, we report the errors $E_{N,\tau}$ and the corresponding temporal convergence orders for scheme (5.9), using the test function (5.11) with parameters $N = 28$, $T = 1$ and $\tau = 1/8, 1/16, 1/32, 1/64, 1/128$. The results clearly demonstrate that the method attains second-order accuracy in time.

Example 2. We adopt the following test function, which is modified from the one proposed in [21]:

$$\begin{cases} u(x,y,t) = \cos(t)\,\sin(\pi x)\,\sin(\pi y)\,e^{-4\pi x^2}\,e^{-4\pi y^2}, \\ v(x,y,t) = -2\cos(t)\,\sin(\pi x)\,\sin(\pi y)\,e^{-4\pi x^2}\,e^{-4\pi y^2}. \end{cases} \tag{5.12}$$

To further illustrate the sharp-gradient behavior of the exact solution (5.12), we extract two one-dimensional slices along the diagonal directions of the square domain, namely

$$\Gamma_1 = \{(x,y)\ :\ x = y\}, \qquad \Gamma_2 = \{(x,y)\ :\ x = -y\}.$$

In Figure 1, we plot the profiles of $u(x,y,0)$, $u(x,y,0)|_{\Gamma_1}$ and $u(x,y,0)|_{\Gamma_2}$. Profile (a) shows that there are two sharp positive peaks and two sharp negative peaks near the origin $(0,0)$. This indicates that the function oscillates vigorously near the origin. Profile (b) shows that the slice decays rapidly around the two positive peaks, while profile (c) indicates that the slice increases rapidly around the two negative peaks. Together, these profiles highlight the sharp gradients near the origin and the fast decay away from the peaks.

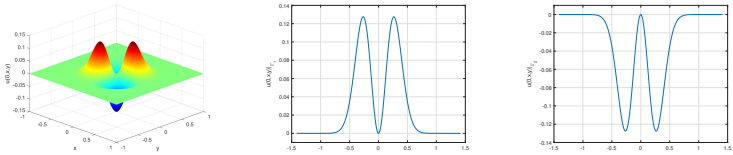

(a) $u(x,y,0)$ (b) $u(x,y,0)|_{\Gamma_1}$ (c) $u(x,y,0)|_{\Gamma_2}$

Figure 1. Solution (5.12) and its two slices at $t=0$.

Figure 2 shows that the errors decay rapidly as N increases and τ decreases. For a fixed τ, the numerical errors are dominated by the spatial approximation error and therefore decrease rapidly as N grows. However, when N becomes sufficiently large, the total numerical error is dominated by the temporal approximation error and thus no longer decreases with increasing N. In this regime, the curves exhibit a second-order convergence rate in time. Figure 3 illustrates that the errors vary between $3.67E-08$ and $5.86E-08$ as the computation time increases, indicating the stability of the long-time simulation. Moreover, these results demonstrate that the proposed algorithm performs well for problems involving sharp gradients.

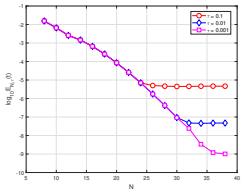

Figure 2. Errors $\log_{10} E_{N,\tau}(t)$ versus the modes N of test function (5.12) with $T=1$, $du=1$, $dv=1$, $F=1$, $k=1$, and $\tau=0.1,0.01,0.001$.

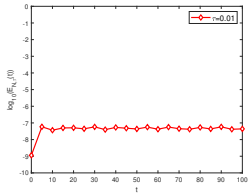

Figure 3. Errors $log_{10}E_{N,\tau}(t)$ of test function (5.12) with $N=32$, $\tau=0.01$, $d_u=1$, $d_v=1$, $F=1$, $k=1$ and $0\le t\le 100$.

Example 3. We choose the test function:

$$\begin{cases} u(x,y,t) = \sin(t+\dfrac{\pi}{2})\sin(2\pi x)^2\sin(2\pi y)^2, \\ v(x,y,t) = \sin(t+\dfrac{\pi}{2})\sin(2\pi x)^2\sin(2\pi y)^2. \end{cases} \tag{5.13}$$

Figure 4 shows that the numerical errors decrease rapidly as the number of modes N increases and the time step τ decreases. For a fixed time step (e.g.,

$\tau = 0.001$), the errors exhibit exponential decay with respect to N over an appropriate range (e.g., $N \leq 26$). When N exceeds this range (e.g., $N > 26$), the error reduction becomes significantly slower or even stagnates, as the total error is then dominated by the temporal discretization error. Moreover, the curves clearly demonstrate a second-order convergence rate in time.

Figure 5 shows that the errors vary between $8.0E-9$ and $6.0E-6$ over the computational time interval $0 \leq t \leq 100$. This indicates the stability of the long-time computation.

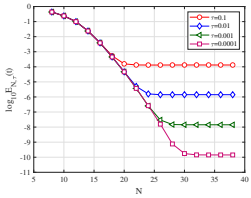

Figure 4. Errors $log_{10}E_{N,\tau}(t)$ versus the modes N of test function (5.13) with $T = 1$, $d_u = 1$, $d_v = 1$, $F = 1$, $k = 1$ and various τ.

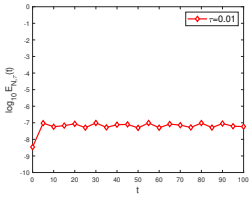

Figure 5. Errors $log_{10}E_{N,\tau}(t)$ of test function (5.13) with $N = 28$, $\tau = 0.01$, $d_u = 1$, $d_v = 1$, $F = 1$, $k = 1$ and $0 \leq t \leq 100$.

To provide a meaningful comparison with existing numerical schemes, we consider a classical finite difference (FD) method. Specifically, a second-order central difference scheme with spatial mesh size h is employed for the spatial discretization, while the backward Euler method with time step τ is used for the temporal discretization. The time step is chosen such that $\tau = \mathcal{O}(h^2)$, which ensures an overall convergence order of $\mathcal{O}(h^2)$ for the FD scheme. The two components of the numerical solution are denoted by $u_{h,\tau}$ and $v_{h,\tau}$, respectively. The errors are measured by the following discrete L^∞-error norm:

$$\tilde{E}_{N,\tau}(t) = \max_{0\leq m\leq N} \max_{0\leq n\leq N} \left\{ |\boldsymbol{v}(x_m, y_n, t) - \boldsymbol{v}_{h,\tau}(x_m, y_n, t)| \right\}.$$

Example 4. We consider the following test function, which is a modified version of the one given in [18]:

$$\begin{cases} u(t,x,y) = \left(e^{-(F+d_u)t} + e^{-(k+d_u)t}\right) \cos(2\pi xy)\,(1-x^2)^2\,(1-y^2)^2, \\ v(t,x,y) = (F-k)\,e^{-(F+d_u)t}\,\cos(2\pi xy)\,(1-x^2)^2\,(1-y^2)^2. \end{cases} \tag{5.14}$$

In Table 2, we report the discrete L^∞-errors $E_{N,\tau}(t)$, $\tilde{E}_{N,\tau}(t)$, and the CPU times (in seconds) versus the modes N for the setting $T = 1$, $d_u = 1$, $d_v = 1$, $F = 1$, and $k = 0.1$, using the SG method with $\tau = 0.01$ and the FD method. The SG method exhibits exponential convergence as the number of modes N increases, whereas the finite difference (FD) method shows only algebraic convergence. For example, to achieve an accuracy of approximately 10^{-5}, the SG method requires only $N = 12$ modes, while the FD method requires $N = 224$. The corresponding CPU times are 0.7802 seconds for the

SG method and $3.0106E+04$ seconds for the FD method. These results clearly demonstrate that the SG method significantly outperforms the FD method in both accuracy and computational efficiency.

Table 2. Errors and CPU times for SG and FD methods versus varying N with test function (5.14).

N	Errors		CPU time (s)	
	$E_{N,\tau}$	$\tilde{E}_{N,\tau}$	SG	FD
8	4.4348E-03	2.3077E-02	0.2990	0.3445
10	4.3922E-04	1.5351E-02	0.4511	0.9263
12	3.0409E-05	9.8306E-03	0.7802	1.8621
14	8.4330E-06	7.5949E-03	1.4100	3.3688
16	8.4566E-06	5.5574E-03	3.4340	5.1795
18	8.4589E-06	4.5628E-03	6.5547	7.9204

Example 5. We choose the initial state as (cf. [11]):

$$u(x,y,0) = 1 - 2v(x,y,0),$$
$$v(x,y,0) = \begin{cases} \frac{1}{4}\sin^2(4\pi x)\sin^2(4\pi y), & \text{if } -\frac{1}{4} \le x,y \le \frac{1}{4}, \\ 0, & \text{otherwise.} \end{cases} \tag{5.15}$$

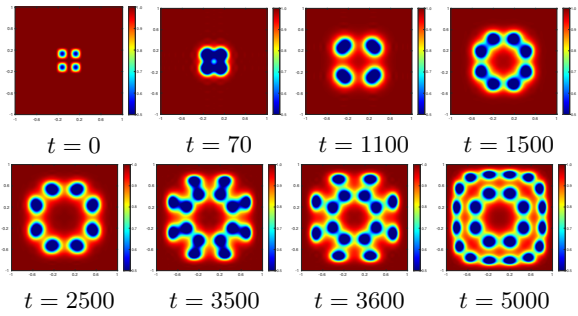

Figure 6. Time evolution of the u-component of the system (3.3), subject to the initial condition (5.15), for the parameter values $N = 32$, $\tau = 0.01$, $d_u = 14 \times 10^{-5}$, $d_v = 7 \times 10^{-5}$, $F = 0.024$, and $k = 0.06$. Snapshots are shown at selected times.

In Figure 6, we plot snapshots of the u-component of (3.3) at selected times over the spatial domain $[-1,1]^2$, using the parameter values specified in the figure caption. Initially, the u-component consists of four spots located near the center of the domain. As time evolves, these spots undergo repeated replication, leading to the formation of a spot pattern throughout the domain.

Example 6. We consider two block functions as the initial condition defined in the domain $[-1,1]^2$ as in [25]:

$$u(x,y,0) = \begin{cases} 0.5, & -0.2 \le x \le 0.2 \text{ and } -0.2 \le y \le 0.2, \\ 1, & \text{otherwise,} \end{cases}$$
$$v(x,y,0) = \begin{cases} 0.25, & -0.2 \le x \le 0.2 \text{ and } -0.2 \le y \le 0.2, \\ 0, & \text{otherwise.} \end{cases} \tag{5.16}$$

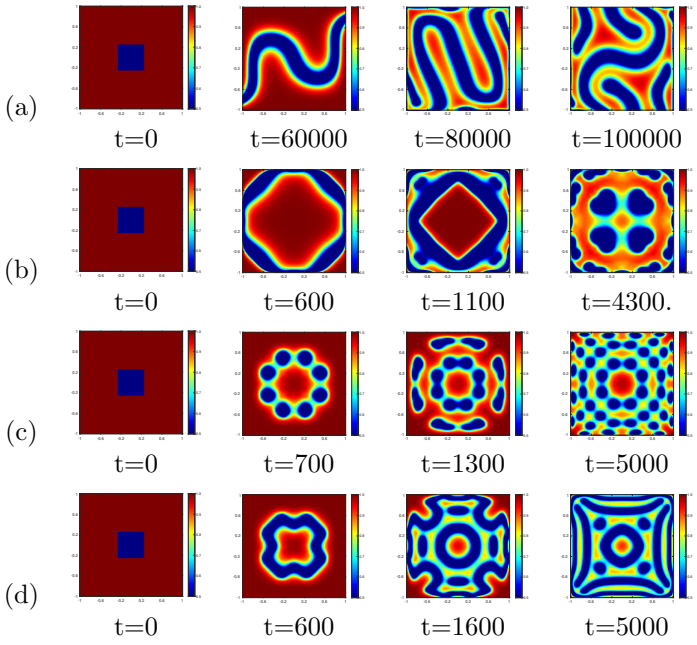

Figure 7. Patterns of the u-component of system (3.3) with initial condition (5.16), computed using $N = 32$ and $\tau = 0.01$. Panels (a)–(b) show the pattern evolution at selected times for different parameter sets: (a) $F = 0.05$, $k = 0.064$, $d_u = 4 \times 10^{-4}$, $d_v = 2 \times 10^{-4}$; (b) $F = 0.02$, $k = 0.05$, $d_u = 1.2 \times 10^{-4}$, $d_v = 6 \times 10^{-5}$. (c) $F = 0.02$, $k = 0.056$, $d_u = 1.2 \times 10^{-4}$, $d_v = 6 \times 10^{-5}$; (d) $F = 0.024$, $k = 0.056$, $d_u = 1.2 \times 10^{-4}$, $d_v = 6 \times 10^{-5}$.

Figure 7 clearly illustrates the pattern dynamics for different choices of the parameter pair (F, k). In panel (a), a stripe-like pattern corresponding to $(F, k) = (0.05, 0.064)$ is observed, which converges to its steady state more slowly than the other patterns. In panel (b), for $(F, k) = (0.02, 0.05)$, no steady stripe or spot pattern is formed; instead, a chaotic pattern emerges, exhibiting certain symmetry properties. In panel (c), a spot-like pattern associated with $(F, k) = (0.02, 0.056)$ develops and converges to a steady state more rapidly. Finally, panel (d) shows a mixed stripe–spot pattern for $(F, k) = (0.024, 0.056)$, which also reaches its steady state relatively quickly. The underlying mechanisms of pattern formation are discussed in [15, 20].

6 Conclusions

In this paper, we proposed a numerical approach for the two-dimensional GS model by combining the spectral-Galerkin method in space with the BDF2 scheme in time. We introduce a class of generalized Jacobi polynomials, two-dimensional projection for vector functions and some related approximation results. We construct a spectral scheme with detailed proofs of the boundedness, the generalized stability, and the convergence. Abundant numerical results demonstrate the spectral convergence rate in space, the stability of long-time computation, and coincide with the theoretical analysis. This new approach

has several advantages: (i) The use of the generalized Jacobi polynomials brings great convenience to analyze the error and leads to a sparse discrete system which can be inverted efficiently. (ii) The numerical solution achieves spectral accuracy in space. The approximation results and the techniques developed in this article are also applicable to other nonlinear systems.

Acknowledgements

The work is supported in part by Nature Science Fundation of China grants No. 12271365, 11771299, and Nature Science Fundation of Shanghai grants No. 22ZR1445400, 20JC1413800.

References

[1] M. Abbaszadeh and M. Dehghan. A reduced order finite difference method for solving space-fractional reaction-diffusion systems: The Gray-Scott model. *Eur. Phys. J. Plus*, **134**:620, 2019. https://doi.org/10.1140/epjp/i2019-12951-0.

[2] M. Abbaszadeh, M. Dehghan and I.M. Navon. A POD reduced-order model based on spectral Galerkin method for solving the space-fractional Gray-Scott model with error estimate. *Eng. Comput.*, **38**:2245–2268, 2022. https://doi.org/10.1007/s00366-020-01195-5.

[3] A.A.A. Amin and D.S. Mashat. Analysis of Gray-Scott's model numerically. *Amer. J. Comput. Math.*, **11**:273–288, 2021. https://doi.org/10.4236/ajcm.2021.114018.

[4] R. Castelli. Rigorous computation of non-uniform patterns for the 2-dimensional Gray-Scott reaction-diffusion equation. *Acta Appl. Math.*, **151**:27–52, 2017. https://doi.org/10.1007/s10440-017-0101-x.

[5] M. Dehghan and M. Abbaszadeh. Numerical study of three-dimensional Turing patterns using a meshless method based on moving Kriging element free Galerkin (EFG) approach. *Comput. Math. Appl.*, **72**:427–454, 2016. https://doi.org/10.1016/j.camwa.2016.04.038.

[6] I.R. Epstein and J.A. Pojman. *An introduction to nonlinear chemical dynamics: oscillations, waves, patterns, and chaos*. Oxford University Press, New York, 1998. https://doi.org/10.1093/oso/9780195096705.001.0001.

[7] P. Gray and S.K. Scott. Autocatalytic reaction in the isothermal, continuous stirred tank reactor: Oscillations and instabilities in the system $a + 2b \to 3b$; $b \to c$. *Chem. Eng. Sci.*, **39**(6):1087–1097, 1984. https://doi.org/10.1016/0009-2509(84)87017-7.

[8] B. Guo, J. Shen and L. Wang. Generalized Jacobi polynomials/functions and their applications. *Appl. Numer. Math.*, **59**(5):1011–1028, 2009. https://doi.org/10.1007/s10915-005-9055-7.

[9] B. Guo, J. Shen and C. Xu. Spectral and pseudospectral approximations using Hermite functions: application to the Dirac equation. *Adv. Comput. Math.*, **19**:35–55, 2003. https://doi.org/10.1023/A:1022892132249.

[10] B. Guo, T. Sun and C. Zhang. Jacobi and Laguerre quasi-orthogonal approximation and related interpolations. *Math. Comp.*, **82**(281):413–441, 2013. https://doi.org/10.1090/S0025-5718-2012-02614-7.

[11] W. Hundsdorfer and J.G. Verwer. *Numerical Solution of Time-Dependent Advection-Diffusion-Reaction Equations*. Springer, Berlin, Heidelberg, 2010. https://doi.org/10.1007/978-3-662-09017-6.

[12] T. Kolokolnikov, M.J. Ward and J. Wei. Zigzag and breakup instabilities of stripes and rings in the two-dimensional Gray–Scott model. *Stud. Appl. Math.*, **116**:35–95, 2006. https://doi.org/10.1111/j.1365-2966.2005.0333.x.

[13] S. Kondo and T. Miura. Reaction-diffusion model as a framework for understanding biological pattern formation. *Science*, **329**:1616–1620, 2010. https://doi.org/10.1126/science.1179047.

[14] J.S. McGough and K. Riley. Pattern formation in the Gray–Scott model. *Nonlinear Anal. Real World Appl.*, **5**:105–121, 2004. https://doi.org/10.1016/S1468-1218(03)00020-8.

[15] A. Munteanu and R.V. Solé. Pattern formation in noisy self-replicating spots. *Int. J. Bifurc. Chaos*, **16**(12):3679–3685, 2006. https://doi.org/10.1142/S0218127406017063.

[16] J.D. Murray. *Mathematical Biology II: Spatial Models and Biomedical Applications*. Springer, New York, NY, 2003. https://doi.org/10.1007/b98869.

[17] Y. Nishiura and D. Ueyama. A skeleton structure of self-replicating dynamics. *Physica D*, **130**:73–104, 1999. https://doi.org/10.1016/S0167-2789(99)00010-X.

[18] S. Singh, R.C. Mittal, S.R. Thottoli and M. Tamsir. High-fidelity simulations for Turing pattern formation in multi-dimensional Gray–Scott reaction-diffusion system. *Appl. Math. Comput.*, **452**:128079, 2023. https://doi.org/10.1016/j.amc.2023.128079.

[19] T. Sun and B. Guo. Generalized Jacobi approximation in multiple dimensions and its applications. *J. Sci. Comput.*, **55**:327–350, 2013. https://doi.org/10.1007/s10915-012-9633-4.

[20] S.A.M. Tonekaboni and A. Shademani. Mathematical investigation of two dimensional pattern formation. *Int. J. Biol. Res.*, **2**(1):1–5, 2014. https://doi.org/10.14419/ijbr.v2i1.1502.

[21] L. Wang and J. Shen. Error analysis for mapped Jacobi spectral methods. *J. Sci. Comput.*, **24**(2):183–218, 2005. https://doi.org/10.1007/s10915-004-4613-y.

[22] W. Wang, Y. Lin, F. Yang, L. Zhang and Y. Tan. Numerical study of pattern formation in an extended Gray-Scott model. *Commun. Nonlinear Sci. Numer. Simul.*, **16**:2016–2026, 2011. https://doi.org/10.1016/j.cnsns.2010.09.002.

[23] J. Wei and M. Winter. Existence and stability of multiple-spot solutions for the Gray–Scott model in r^2. *Physica D*, **176**:147–180, 2003. https://doi.org/10.1016/S0167-2789(02)00743-1.

[24] O.P. Yadav and R. Jiwari. A finite element approach for analysis and computational modelling of coupled reaction diffusion models. *Numer. Methods Partial Differential Equations*, **35**:830–850, 2019. https://doi.org/10.1002/num.22328.

[25] P.A. Zegeling and H.P. Kok. Adaptive moving mesh computations for reaction–diffusion systems. *J. Comput. Appl. Math.*, **168**:519–528, 2004. https://doi.org/10.1016/j.cam.2003.06.013.